Carrier-confinement effects in nanocolumnar GaN/$Al_xGa_{1-x}N$ quantum disks grown by molecular-beam epitaxy

Jelena Ristić,* Carlos Rivera, Enrique Calleja, and Sergio Fernández-Garrido
ISOM and Departamento de Ingeniería Electrónica, Universidad Politécnica, Madrid, Spain

Michael Povoloskyi and Aldo Di Carlo
Dipartimento di Ingegneria Elettronica, Universita di Roma "Tor Vegata", Roma, Italy
(Received 4 February 2005; revised manuscript received 4 May 2005; published 16 August 2005)

Carrier confinement effects in nanocolumnar $Al_xGa_{1-x}N$/GaN multiple quantum disks have been studied by photoluminescence, as a function of the Al content and quantum disk thickness. Experimental emission energies are compared to theoretical calculations based on a one-dimensional Schrödinger-Poisson solver, including spontaneous and piezoelectric polarizations, surface potentials, and strain. An inhomogeneous biaxial (in-plane) strain distribution within the GaN quantum disks, pseudomorphically grown on strain-free $Al_xGa_{1-x}N$ nanocolumns, results from a reduction of the accumulated elastic energy at the disk free surface (GaN-air boundary). This strain reduction annihilates partially the piezoelectric field, giving rise to a specific carrier confinement mechanism (*strain confinement*), that depends on the disk thickness. This *strain confinement* mechanism is the origin of the luminescence quenching in very thin GaN quantum disks, as well as the main source of the emission linewidth broadening.

DOI: 10.1103/PhysRevB.72.085330 PACS number(s): 78.67.Bf, 77.65.Ly, 81.16.Dn, 78.67.De

I. INTRODUCTION

Nanoscale semiconductor heterostructures emerge as the most promising approach to improve the performance of optoelectronic devices (light-emitting diodes and lasers), and to develop a whole range of new devices for broadband (UV to IR) radiation- and bio-sensing, single-photon-sources, and wavelength tunable optical switches.[1–4] Self-organized III-nitride nanocolumns, with exceptional crystal quality, were grown by molecular beam epitaxy (MBE).[5–8] Arrays of such nanostructures may be integrated into larger scale devices, without additional processing (patterning, etching).

In spite of the increasing number of reports on the growth of nitride nanocolumns, detailed studies on their optical properties are very scarce,[7,9] and a deeper comprehension of the physical mechanisms governing the optical and electrical behavior of these structures is needed. Given the rather high carrier effective masses and the typical nanocolumn diameters (20–120 nm), quantum effects are not likely to manifest in simple nanocolumns. However, nanocolumnar heterostructures including quantum disks (QDisks) bring new effects ensuing from quantum confinement, strain distribution, and piezoelectric fields. The novelty in these structures is twofold: on one hand, the material system and the nanoscale dimensions in a columnar geometry. On the other hand, the close relation among strain, piezoelectric field, and potential confinement that offers in such heterostructures a very interesting phenomenon from a point of view of basic physics.

This work focuses on the optical properties of $Al_xGa_{1-x}N$ nanocolumnar heterostructures comprising multiple GaN quantum disks (MQDisks). Photoluminescence (PL) was excited with a second-harmonic generator pumped by Ar^+ laser (257 nm), dispersed by a Jobin-Yvon THR 100 monochromator, and detected with an UV-enhanced GaAs photomultiplier. PL spectra, as a function of the Al content and the MQDisks thickness, are compared with simulated results that consider spontaneous and piezoelectric polarization, surface potentials, and screening effects.

II. EXPERIMENT

Reference $Al_xGa_{1-x}N$ nanocolumnar samples, with nominal Al contents of 20%, 23%, and 28%, were grown by plasma-assisted MBE (PAMBE) on Si(111) substrates, under N-rich conditions. Subsequently, $Al_xGa_{1-x}N$/GaN nanocolumnar heterostructures were grown including 5 GaN QDisks, 2, 3, and 4 nm thick, separated by 10 nm thick $Al_xGa_{1-x}N$ barrier layers, and capped by a 20 to 50 nm thick $Al_xGa_{1-x}N$ layer. More details on the growth optimization and the experimental setup are given elsewhere.[8,9]

A self-consistent 1D Schrödinger-Poisson solver[10] was used for the band structure simulation and the corresponding wave function modeling. The calculation was performed iteratively using the numerical method of finite differences. Given the small range of Al contents, a linear dependence of the polarization fields on the Al content was assumed. Fully ionized dopants, discretized into 1 Å steps on the numerical space mesh, were added, simulating the polarization charges. Band structure parameters, listed in Table I, were obtained from data in the literature.[11–13] An electron density of 5×10^{17} cm^{-3}, typical for unintentionally doped GaN compact layers, was assumed in the calculations. The Fermi level pinning at the surface was included, considering free-surface potential barriers of 1.5 and 1.7 eV for 20% and 28% Al content $Al_xGa_{1-x}N$ layers (top capping), and around 1 eV for GaN.[14]

Since single $(Al_x)Ga_{1-x}N$ nanocolumns are strain-free,[15] the GaN MQDisks are grown pseudomorphically on the $Al_xGa_{1-x}N$ nanocolumns, thus subjected to biaxial (in-plane)

TABLE I. Parameters used in the simulation (Refs. 11–13). The values for $Al_xGa_{1-x}N$ are taken as a linear interpolation between the respective binary ones.

Wurtzite		GaN	AlN
Energy gap @ 4 K		3.510 eV	6.230 eV
Lattice parameter, a		3.189 Å	3.112 Å
Dielectric constant, ε		9.5 ε_0	8.5 ε_0
Effective masses	electron, m_e^*	0.2 m_0	0.3 m_0
	heavy hole, m_{hh}^*	1.0 m_0	3.5 m_0
	a_{cz}	−6.5 eV	
	$a_{c\perp}$	−11.8 eV	
	D_1	−3 eV	
	D_2	3.6 eV	
	D_3	8.82 eV	
	D_4	−4.41 eV	
Elastic constants	C_{13} [GPa]	106	
	C_{33} [GPa]	398	
Piezoelectric coefficients	e_{13}	−0.35	
	e_{33}	1.27	
Spontaneous polarization (Refs. 12 and 13)		−0.029 C/m^2	−0.035 to −0.05 C/m^2

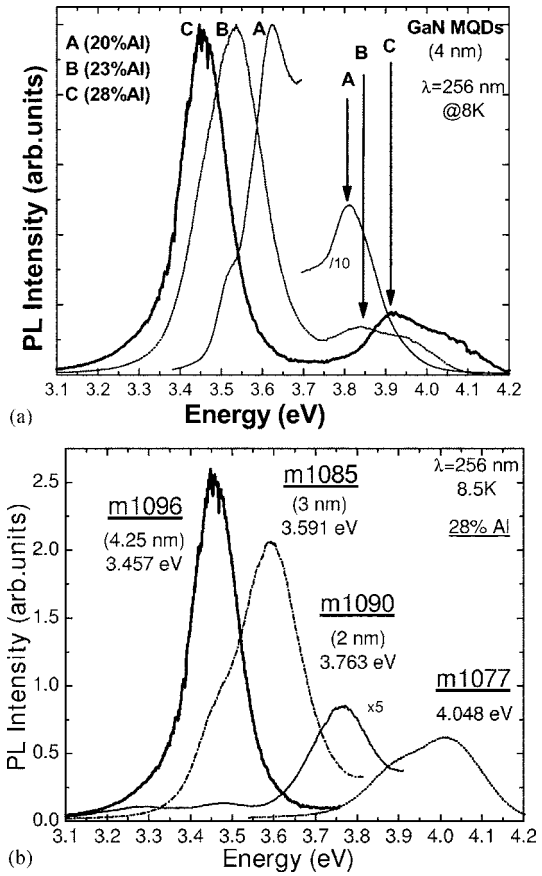

FIG. 1. (a) Photoluminescence spectra of a 5 period, 4 nm thick, GaN MQDisks embedded into $Al_xGa_{1-x}N$ nanocolumns with different Al content. (b) Photoluminescence spectra of a 5 period (2, 3, and 4.2 nm thick) GaN MQDisks embedded in an $Al_{0.28}Ga_{0.72}N$ nanocolumn. PL spectra of the reference $Al_{0.28}Ga_{0.72}N$ nanocolumn sample (m1077) are also shown.

compressive strain. Indeed, transmission electron microscopy (TEM) studies do not reveal strain relaxation of the GaN MQDisks through dislocation formation. However, an inhomogeneous strain distribution is expected within the MQDisks due to their lateral free surface. To quantify the degree of accumulated elastic energy, the strain tensor equation was solved for the in-plane and growth directions and the corresponding boundary conditions.[18]

III. RESULTS AND DISCUSSION

A. Optical characterization

Normalized PL spectra of three nanocolumnar heterostructures, with 4 nm thick GaN MQDisks, but different Al composition in the barriers, are shown in Fig. 1(a). Emissions from the MQDisks at 3.624, 3.534, and 3.456 eV (for 20%, 23%, and 28% Al) are clearly resolved from those of the $Al_xGa_{1-x}N$ barrier layers and the main nanocolumn that appear at higher energies [m1077 in Fig. 1(b)]. The emission from the $Al_xGa_{1-x}N$ in sample *A* is actually stronger, because the nanocolumn height is 5 times that of samples *B* and *C*. A pronounced *redshift* of the GaN MQDisks emissions is observed with increasing Al content. This trend can only be explained in terms of increasing polarization fields within the MQDisks that reinforce the quantum confined Stark effect (QCSE).

A second set of nanocolumnar heterostructures with 28% Al in $Al_xGa_{1-x}N$ layers (main nanocolumn and barriers), and different GaN MQDisks thickness, was studied. PL spectra of samples with 2, 3, and 4.2 nm thick GaN MQDisks are shown in Fig. 1(b). The expected *blueshift* of the GaN MQDisks emission peak with decreasing disk thickness is observed. However, the strong reduction of the emission intensity, observed when decreasing the MQDisks, thickness,

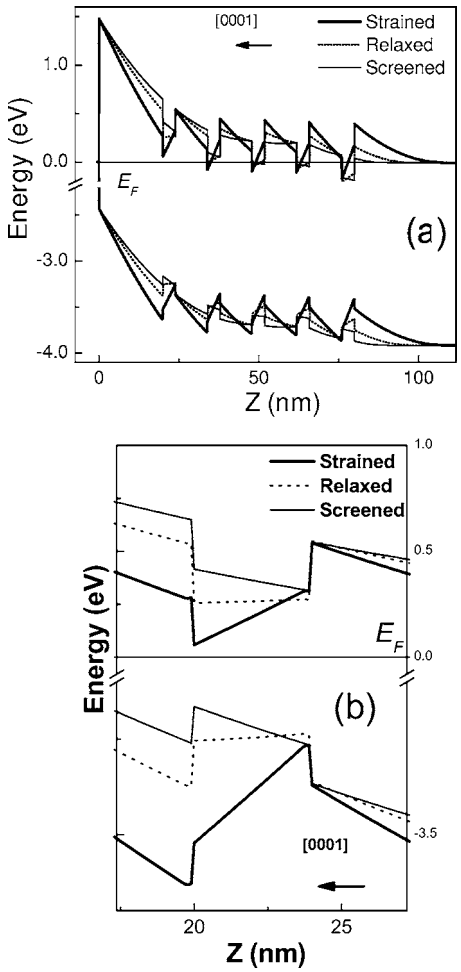

FIG. 2. (a) Band diagram of a GaN MQDisk heterostructure assuming different strain conditions and screening effects. (b) The band structure details for the disk nearest to the top nanocolumn surface.

cannot be easily understood in terms of reduced scattering volume. Results from a self-consistent 1D Schrödinger-Poisson equation solver will show that the strain-dependent band structure within the MQDisks plays a major role to determine the emission energies and their relative intensities.

B. Heterostructure band profiles and wave function simulation

The band potential profile of a heterostructure with 4 nm thick GaN MQDisks, grown on an $Al_{0.2}Ga_{0.8}N$ nanocolumn and capped by a 20 nm thick $Al_{0.2}Ga_{0.8}N$ layer [sample *A* in Fig. 1(a)], was modeled by a self-consistent 1D Schrödinger-Poisson solver along the [0001] direction (nanocolumn height), considering the Fermi level pinned at the top surface. Strain-induced band gap changes were considered, according to the following equations:

$$\frac{\partial E_G}{\partial \varepsilon_{zz}} = [a_{cz} - (D_1 + D_3)] - \frac{C_{33}}{C_{13}}[a_{c\perp} - (D_2 + D_4)]. \quad (1)$$

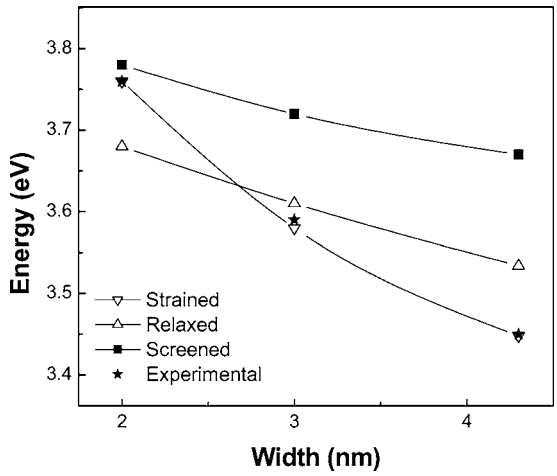

FIG. 3. Experimental [PL data from Fig. 1(b)] and calculated values of the emission energies for the heterostructures with QDisks of different thicknesses.

$$E_G^{strain}(\mathrm{GaN}) = E_G^{relaxed}(\mathrm{GaN}) - \left[\frac{\partial E_G}{\partial \varepsilon_{zz}}\right]\varepsilon_{zz}, \quad (2)$$

where ε_{zz} is the strain along the *c* axis, a_{cz}, $a_{c\perp}$, D_1, D_2, D_3, and D_4 are GaN deformation potential constants, C_{33} and C_{13} are GaN elastic constants (Table I).

Three possible cases are shown in Fig. 2(a). due to the Fermi level pinning at the top surface (Schottky-type barrier).

The first one accounts for both spontaneous and piezoelectric polarizations in fully strained GaN QDisks, which results in a strong electric field within the QDisks opposed to that of the space-charge region (SCR) due to the Fermi level pinning at the top surface. A second one assumes only the spontaneous polarization in fully relaxed GaN QDisks that still yields within the QDisks an electric field in the direction opposite to that of the SCR. A third case considers fully strained GaN QDisks, which are totally screened. Notice that, in this case, the GaN band gap energy corresponds to that of the material under biaxial compressive strain. Figure 2(b) shows in detail the potential profiles of the **first** QDisk (topmost) for the three cases mentioned: fully strained, fully relaxed, and fully screened.

In order to compare the experimental and calculated emission energies from the GaN QDisks as a function of their width, the self-consistent solution of the 1D Schrödinger-Poisson solver, for the whole structure, has been considered. However, the energy values plotted in Fig. 3 correspond to the **fifth** QDisk of sample *A*, which is the one with the highest probability to generate the PL signal. Figure 3 shows the comparison between experimental and theoretical emission energies that fit well in the case of fully strained GaN QDisks, thus, ruling out screening effects as a major factor to determine the QDisk potential profile. The crossing of the calculated energies for the strained and relaxed cases in Fig. 3 is explained in terms of changes in confinement that depend on the GaN QDisk thickness, as it will be shown in the discussion (Sec. III D).

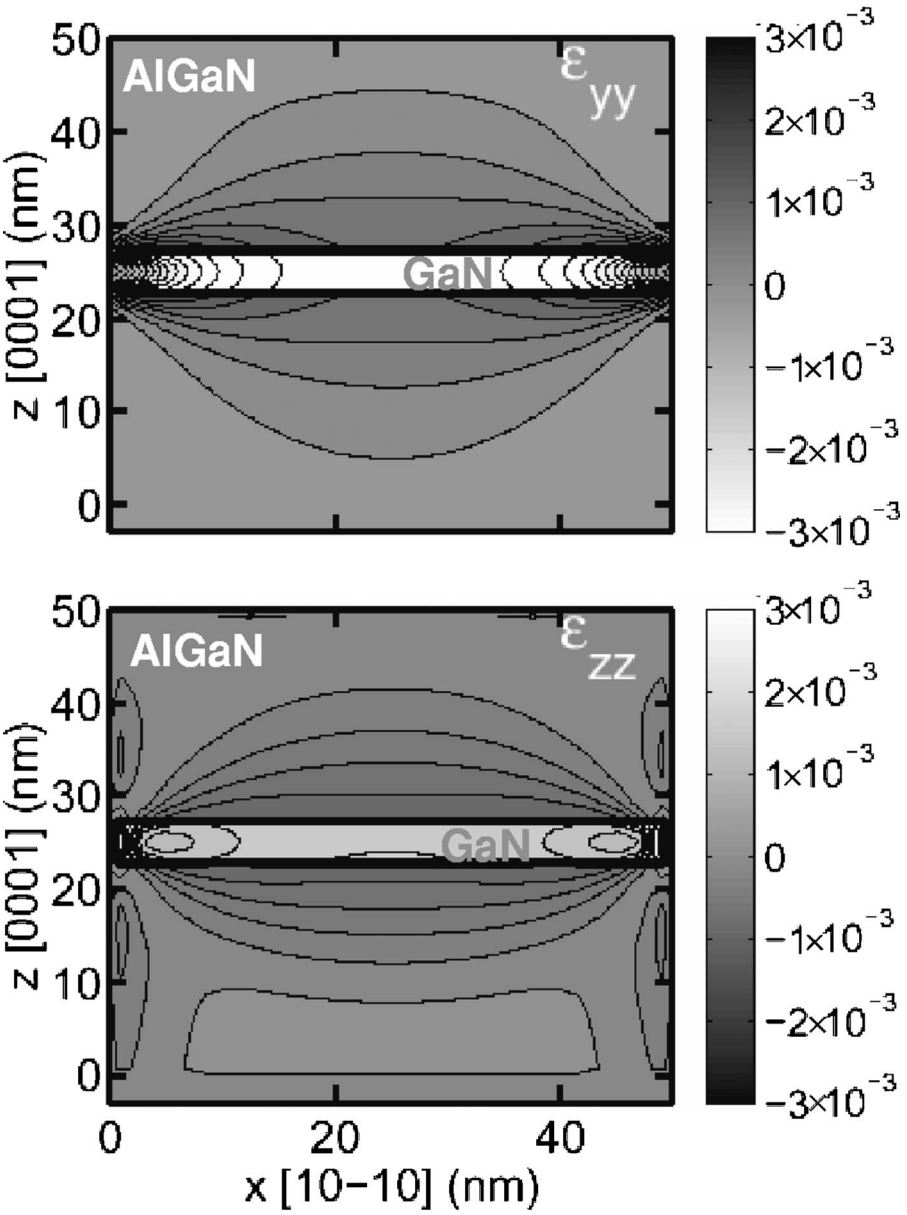

FIG. 4. In-plane (ε_{yy}) and growth direction (ε_{zz}) strain distributions, according to the strain tensor equation solver in GaN QDisks within a homoepitaxially grown $Al_xGa_{1-x}N$ nanocolumn.

C. Inhomogeneous strain distribution within the GaN MQDisks

As mentioned before, single $(Al_x)Ga_{1-x}N$ nanocolumns are strain-free due to relaxation at the substrate interface and to their high surface-to-volume ratio.[15,16] The GaN MQDisks are pseudomorphic to the underlying $Al_xGa_{1-x}N$ nanocolumn, and thus subjected to biaxial (in-plane) compressive strain. High-resolution TEM images do not reveal the presence of threading dislocations or other strain-relieving defects in the GaN MQDisks.[9] Indeed, there is no evidence of such strain-relieving defects even in more complicated nanostructures like an AlN/GaN nanocolumnar Bragg reflector with stacks thicker than 70 nm that would accumulate a much higher strain.[17] Yet, due to the GaN MQDisks lateral free surface, the strain within them is expected to be inhomogeneously distributed.

The equilibrium strain distribution profile of a single 4 nm thick GaN QDisk cladded by $Al_xGa_{1-x}N$ (20% Al) barriers and surrounded by air, is obtained by solving the strain tensor equation[18] using the NEXTNANO3 simulation package.[19] The converse piezoelectric effect is neglected.[20] The resulting in-plane ($\varepsilon_{xx}=\varepsilon_{yy}$) and out-of-plane ($\varepsilon_{zz}$) strain profiles for corresponding boundary conditions, namely, the GaN Qdisks, surrounded by $Al_xGa_{1-x}N$ barriers, grown on a strain-free $Al_xGa_{1-x}N$, are shown in Fig. 4. Resultant GaN disk in-plane lattice parameter variation is represented in Fig. 5. While the GaN QDisk center is almost fully strained (ε_{yy}), there is a continuous relaxation towards the lateral surface, where the strain approaches zero. As a consequence, both the MQDisk internal electric field (piezoelectric component) and the GaN energy gap will vary along the QDisk diameter. Strain may also appear in the $Al_xGa_{1-x}N$ barrier layers, but, given the complexity of the problem, this effect will not be taken into account.

A very relevant issue is that the inhomogeneous nature of the in-plane strain distribution cannot be neglected in the

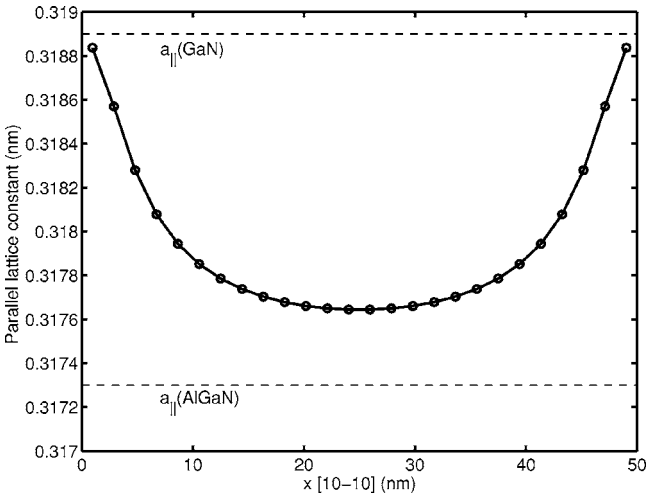

FIG. 5. Variation of the in-plane lattice parameter in 4 nm thick GaN QDisk, according to the strain tensor equation solver.

studied structures, as it affects the carrier confinement through the band gap changes and the potential profile (piezoelectric field).

D. Discussion

This section addresses the effect of the in-plane (lateral) strain distribution within the GaN MQDisks on the PL emissions intensity and linewidth broadening.

Data on the lateral strain distribution within the GaN QDisk in Fig. 4(a) are numerical solutions and, thus, no analytical function describing the strain distribution is available. Changes of the vertical confinement potential, $V(z)$, from the QDisk center to the lateral free surface, are estimated considering two extreme cases along the x axis (one dimension): (i) fully strained GaN at the QDisk center ($x=0$), and (ii) fully relaxed GaN at the lateral free surface ($x=\pm r$, r being the disk radius). The actual shape of the confinement potential between these two points depends on the specific strain variation, which we assume to be a continuous and monotonous function.

The ground-state ($e1$-$hh1$) transition energy, denominated "*GaN effective band gap*" by some authors[21] (E_G^{eff}), is derived from the equations

$$E_G^{eff}(x=0) = E_G^{strained}(\mathrm{GaN}) + E_{conf}^{strained} - eF_{tot}^{strained}w, \quad (3)$$

$$E_G^{eff}(x=r) = E_G^{relaxed}(\mathrm{GaN}) + E_{conf}^{relaxed} - eF_{tot}^{relaxed}w, \quad (4)$$

for the center and the lateral free surface of the QDisk, respectively. E_G^{strain} (GaN) is given by Eq. (2). F_{tot} is the total electric field in the QDisk of thickness w, and the term $eF_{tot}w$ accounts for the QCSE that modifies the carrier confinement.[21] E_{conf} represents the quantum confinement energy for electrons and holes within the QDisk, which, for a triangular shape approximation, depends on the electric field as $F_{tot}^{2/3}$. $E_{conf}^{strained}$ is about twice as high as $E_{conf}^{relaxed}$ for the range of QDisk thicknesses studied.

For thick (4.2 nm) GaN QDisks, the term E_{conf} has a lower weight in Eqs. (3) and (4) compared to $eF_{tot}w$. Even

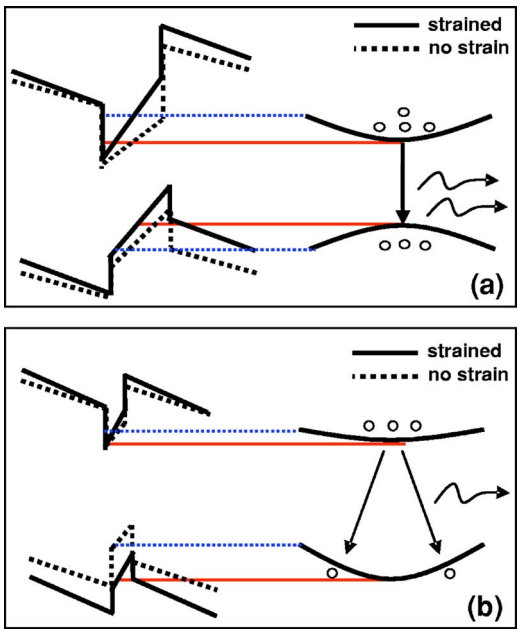

FIG. 6. (Color online) Potential profile (left) and corresponding carrier confinement energy (right) for the center (fully strained) and the free lateral surface (fully relaxed) of (a) thick QDisk; and (b) thin QDisk.

though E_G^{strain} (GaN) is larger than $E_G^{relaxed}$ (GaN), the electric field F_{tot} in the strained region (center) of the GaN QDisk is much larger than that of the relaxed one (lateral free surface), so that $E_G^{eff}(x=r) > E_G^{eff}(x=0)$. In this case, the emission arising from the QDisk periphery will be of a higher energy than that from the center, as it is illustrated in Fig. 6(a), where the continuous line is a guide to the eye, assuming a monotonous and continuous strain variation from the center to the lateral free surface. This potential distribution tends to localize both electrons and holes in the central area of the QDisk with a strong wave function overlap that will give high emission intensity. An increasing carrier population in such a confinement potential will produce an emission energy broadening that depends on the specific potential profile and the carrier spreading within it. An upper limit for this broadening is the difference between the emission energy values from the QDisk center and the lateral free surface, which amounts up to 150 meV for the entire heterostructure.

For thin (2 nm) GaN QDisks, the confinement term, E_{conf}, and the strain-induced energy difference, $\Delta E_G = -[\partial E_G/\partial \varepsilon_{zz}] \times \varepsilon_{zz}$, have a much higher weight in Eqs. (3) and (4) than the polarization field effect, $eF_{tot}w$. As a result, $E_G^{eff}(x=0) > E_G^{eff}(x=r)$, which is opposite to what is found for thick GaN QDisks. In this case, the emission from the QDisk periphery will have a lower energy than that from its center, as shown in Fig. 6(b). The resulting delocalization of electrons and holes gives rise to a much lower emission intensity for very thin QDisks, as observed experimentally [Fig. 1(b)]. An emission energy broadening will also occur in this case, depending on the specific potential profile and the carrier distribution within it.

This rather simple model, derived from the lateral strain distribution within the QDisk, provides a straightforward ex-

planation for the PL emission quenching in very thin QDisks, as well as for the emission energy broadening measured by PL. In this model we have neglected the presence of a surface potential and band bending along the QDisk diameter. The calculated value of this band bending, given the surface potential (1 eV, for GaN), the residual doping, and the QDisk diameter (20–40 nm), is around 25 meV, a value much lower than the confinement potential variations along the QDisk diameter.

Another significant source of emission linewidth broadening is the different potential that individual GaN QDisks endure due to the presence of a top surface potential and the subsequent development of a vertical SCR (from the top of the nanocolumn), as shown in Fig. 2(a). In order to estimate this effect, we have calculated the emission energy value for the *first* and the *fifth* QDisk, assuming that they are pseudomorphic (fully strained), for heterostructures with 50 and 20 nm $Al_xGa_{1-x}N$ cap layer. The results obviously depend on the cap layer thickness, yielding 20 to 150 meV for the two cap layer thicknesses considered. These values may in the worst case add up to the broadening generated within a single QDisk mentioned before.

IV. CONCLUSIONS

In summary, a detailed optical characterization of nanocolumnar $Al_xGa_{1-x}N/GaN$ MQDisk heterostructures has been performed, taking into account spontaneous and piezoelectric polarizations, surface potentials, screening effects, and a lateral inhomogeneous strain distribution within the QDisks. This inhomogeneous strain distribution along the QDisk diameter leads to a specific confinement potential (*strain confinement*) that depends strongly on the QDisk thickness. For rather thick QDisks, carriers are localized at the disk center, providing a strong electron-hole wave function overlap and, consequently, intense emissions. For thin QDisks, the confinement potential delocalizes spatially electrons and holes within the disk, thus, leading to a very strong reduction of the emission intensity (quenching). Two main sources of emission linewidth broadening are identified. One is due to the confinement potential within each individual QDisk, whereas a second one derives from the presence of a surface potential at the nanocolumn top surface that develops into a SCR electric field that affects the various QDisks in the heterostructure differently.

ACKNOWLEDGMENTS

Partial financial support was provided by Spanish ministry of Education and Science Project No. MAT-2004-02875, Autonomous Community of Madrid Project No. GR/MAT/0042/2004, and European Project MRTN-CT-2003-503677 "CLERMONT II".

*Permanent address: Departamento de Ciencias de la Comunicación, Universidad Rey Juan Carlos, 28943 Fuenlabrada, Madrid Spain. Email addresses: jelena@die.upm.es, jelena.ristic@urjc.es

[1] Y. Arakawa and H. Sakaki, Appl. Phys. Lett. **40**, 939 (1982).
[2] K. Hiruma M. Yazawa, T. Katsuyama, K. Ogawa, K. Haraguchi, M. Koguchi, and H. Kakibayashi, J. Appl. Phys. **77**, 447 (1995), L. Samuelson, *Materials Today* (Elsevier, New York, 2003).
[3] J. Shakya, K. H. Kim, J. Li, J. Y. Lin, and H. X. Jiang, Mater. Res. Soc. Symp. Proc. **798**, Y4.6.1 (2004).
[4] E. Moreau, I. Robert, J. M. Gérard, I. Abram, L. Manin, and V. Thierry-Mieg, Appl. Phys. Lett. **79**, 2865 (2001).
[5] M. Yoshizawa, A. Kikuchi, N. Fujita, K. Kushi, H. Sasamoto, and K. Kishino, J. Cryst. Growth **189/190**, 138 (1998).
[6] S. Guha, N. Bojarczuk, M. Johnson, and J. Schetzina, Appl. Phys. Lett. **75**, 463 (1999).
[7] E. Calleja, M. A. Sánchez-García, F. J. Sánchez, F. Calle, F. B. Naranjo, E. Muñoz, U. Jahn, and K. Ploog, Phys. Rev. B **62**, 16826 (2000).
[8] J. Ristić, M. A. Sánchez-García, E. Calleja, J. Sánchez-Páramo, J. M. Calleja, U. Jahn, and K. H. Ploog, Phys. Status Solidi A **192**, 60–66 (2002).
[9] J. Ristić, E. Calleja, M. A. Sánchez-García, J. M. Ulloa, J. Sánchez-Páramo, J. M. Calleja, A. Trampert, U. Jahn, and K. H. Ploog, Phys. Rev. B **68**, 125305 (2003).
[10] G. Snider, 1D Poisson/Schrödinger, http://www.nd.edu/~gsnider/; Electronic mail: snider.7@nd.edu (1997).
[11] I. Vurgaftman, J. R. Meyer, and L. R. Ram-Mohan, J. Appl. Phys. **89**, 5815 (2001).
[12] N. Grandjean, B. Damilano, S. Dalmasso, M. Leroux, M. Laügt, and J. Massies, J. Appl. Phys. **86**, 3714 (1999).
[13] M. Leroux, N. Grandjean, J. Massies, B. Gil, P. Lefebvre, and P. Bigenwald, Phys. Rev. B **60**, 1496 (1999).
[14] S. Sabuktagin, M. A. Reshchikov, D. K. Johnstone, and H. Morkoç, Mater. Res. Soc. Symp. Proc. **798**, Y.5.39 (2004).
[15] J. Sánchez-Páramo, J. M. Calleja, M. A. Sánchez-García, E. Calleja, and U. Jahn, Physica E (Amsterdam) **13**, 1070 (2002).
[16] A. Trampert, J. Ristić, U. Jahn, E. Calleja, and K. H. Ploog, in Proceedings of the 13th International Conference on Microscopy of Semiconducting Materials, edited by A. G. Cullis and P. A. Midgley, IOP Conf. Ser. No. 180, 167 (2003).
[17] J. Ristić, E. Calleja, A. Trampert, S. Fernández-Garrido, C. Rivera, U. Jahn, and K. H. Ploog, Phys. Rev. Lett. **94**, 146102 (2005).
[18] J. F. Nye, *Physical Properties of Crystals* (Oxford University Press, Oxford, 1957).
[19] http://icode.eln.uniroma2.it
[20] E. Pan, J. Appl. Phys. **91**, 3785 (2002).
[21] A. Bonfiglio, M. Lomascolo, G. Traetta, R. Cingolani, A. Di Carlo, F. Della Sala, P. Lugli, A. Botchkarev, and H. Morkoc, J. Appl. Phys. **87**, 2289 (2000); A. Hangleiter, J. Lumin. **87–89**, 130 (2000).